Stoichiometric Effect on Electrical, Optical, and Structural Properties of Composition-Tunable $In_xGa_{1-x}As$ Nanowires

Jared J. Hou,[†] Fengyun Wang,[†] Ning Han,[†] Fei Xiu,[†] SenPo Yip,[†] Ming Fang,[†] Hao Lin,[†] Tak F. Hung,[†] and Johnny C. Ho[†,‡,*]

[†]Department of Physics and Materials Science and [‡]Centre of Functional Photonics (CFP), City University of Hong Kong, Tat Chee Avenue, Kowloon, Hong Kong SAR, China

ABSTRACT

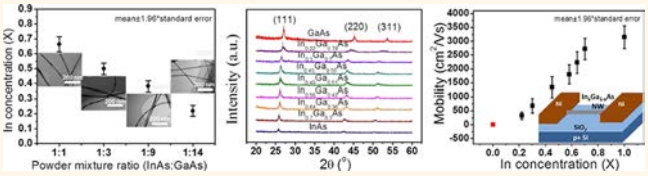

Ternary InGaAs nanowires have recently attracted extensive attention due to their superior electron mobility as well as the ability to tune the band gap for technological applications ranging from high-performance electronics to high-efficiency photovoltaics. However, due to the difficulties in synthesis, there are still considerable challenges to assess the correlation among electrical, optical, and structural properties of this material system across the entire range of compositions. Here, utilizing a simple two-step growth method, we demonstrate the successful synthesis of composition and band gap tunable $In_xGa_{1-x}As$ alloy nanowires (average diameter = 25−30 nm) by manipulating the source powder mixture ratio and growth parameters. The lattice constants of each NW composition have been well correlated with the chemical stoichiometry and confirmed by high-resolution transmission electron microscopy and X-ray diffraction. Importantly, the as-grown NWs exhibit well-controlled surface morphology and low defect concentration without any phase segregation in all stoichiometric compositions. Moreover, it is found that the electrical nanowire device performances such as the turn-off and I_{ON}/I_{OFF} ratios are improved when the In concentration decreases at a cost of mobility degradation. More generally, this work suggests that a careful stoichiometric design is required for achieving optimal nanowire device performances.

KEYWORDS: indium gallium arsenide · nanowires · two-step growth method · stoichiometry · composition tunable · field-effect mobility

Due to their unique physical properties, semiconductor nanowires (NWs) have attracted enormous attention as promising active materials for future electronic[1,2] and optoelectronic devices.[3,4] In particular, ternary alloy NWs have been demonstrated to create a uniform stoichiometric system that can be synthesized with facile growth methods without introducing complex heterojunctions.[5,6] They also offer a great flexibility of tunable band gap by changing the relative composition of their alloys such as $In_xGa_{1-x}N$ (1.12−3.43 eV),[7] $Al_xGa_{1-x}N$ (3.4−6.2 eV),[8] and CdS_xSe_{1-x} (1.73−2.44 eV),[9] which is advantageous for various device structures.[10−13] Recently, indium gallium arsenide ($In_xGa_{1-x}As$) NWs have become of great interest due to their variable band gap, spanning from the near-infrared to the infrared region (0.34−1.42 eV).[14−16] In addition to the benefits arising from this tunable band gap in photovoltaics,[17] the electrical properties of $In_xGa_{1-x}As$ NWs could also be modulated as needed in lowering the off-state leakage current while maintaining a high electron mobility in electronic devices. Despite the success in the synthesis of completely tunable compositions,[18] important relationships among the electrical, optical, and structural properties and chemical composition in this NW material system still have not been well studied until now. Understanding all of this would be essential to design and implement $In_xGa_{1-x}As$ NWs for more advanced technological applications.

In this study, we present the synthesis of composition-tunable $In_xGa_{1-x}As$ NWs by a simple two-step growth method and correlate the electrical, optical, and structural properties with the NW stoichiometry. The experimental results illustrate a well-controlled, uniform growth of single-crystalline NWs with a smooth surface and low defect concentration for all stoichiometric compositions. X-ray diffraction (XRD) and UV−vis optical absorption measurements confirm the complete composition tuning and band gap engineering over the entire range for the material system. More importantly, the

* Address correspondence to johnnyho@cityu.edu.hk.

Received for review September 10, 2012 and accepted September 28, 2012.

Published online September 28, 2012
10.1021/nn304174g

electrical properties of $In_xGa_{1-x}As$ NWs, when configured as back-gated field-effect transistors (FETs), reveal composition-dependent behaviors. Specifically, decreasing the In content of NWs would increase the band gap and I_{ON}/I_{OFF} ratio, but this is attained at the cost of electron mobility degradation. All of this suggests that a careful device design consideration manipulating the ternary NW composition and electrical properties is required to achieve optimal device performances.

RESULTS AND DISCUSSION

The $In_xGa_{1-x}As$ NWs used in this study were synthesized by a two-step catalytic chemical vapor deposition (CVD) method previously reported.[19] In order to produce the complete composition-tunable NWs, different ratios of InAs and GaAs source powder were used, *e.g.*, InAs:GaAs = 1:1, 1:3, 1:9, and 1:14 in weight ratio. This mixture ratio predetermined the available vapor pressure of In and Ga precursors under a specific source temperature; therefore, it has a significant influence on the final composition of the grown ternary NWs. As shown in Figure 1a, the In concentration of as-grown NWs decreases with the In content in a predetermined mixture, while the composition of NWs was determined by energy-dispersive X-ray spectroscopy (EDS). For example, for each mixture ratio, around 30 NWs were randomly chosen as candidates for the EDS point scan in the NW body to statistically determine the composition (see Supporting Information Figure S1 for representative EDS spectra). The 95% confidence interval for the average composition is also depicted by the error bar for each mixture, demonstrating the tight control over the NW stoichiometry with this simple powder mixing technique. Notably, this tunability covers almost the entire composition range of $In_xGa_{1-x}As$ ($0.2 < x < 0.75$) and could be further refined by tuning the powder mixture ratio. Furthermore, during the growth, a two-step method is utilized to optimize the NW growth yield and morphology. As previously reported, this method can significantly reduce the kinked morphology and surface coating in In-rich InGaAs NWs, while in this study, by carefully adjusting the growth parameters, such as nucleation temperature, growth temperature, and growth time, as-grown NWs can have the desirable morphology in all composition ranges. As demonstrated in Figure 1b–e, $In_{0.64}Ga_{0.36}As$, $In_{0.45}Ga_{0.55}As$, $In_{0.3}Ga_{0.7}As$, and $In_{0.22}Ga_{0.78}As$ NWs all exhibit a smooth surface and nontapered characteristics along the entire NW length, favoring subsequent device fabrication and performance. Also, the NW density of each composition range is sufficient (>10 μm^2) for large-scale assembly (see Supporting Information Figure S2) by the contact printing method and is promising to produce spatially composition-graded InGaAs NW arrays. More importantly, the diameter

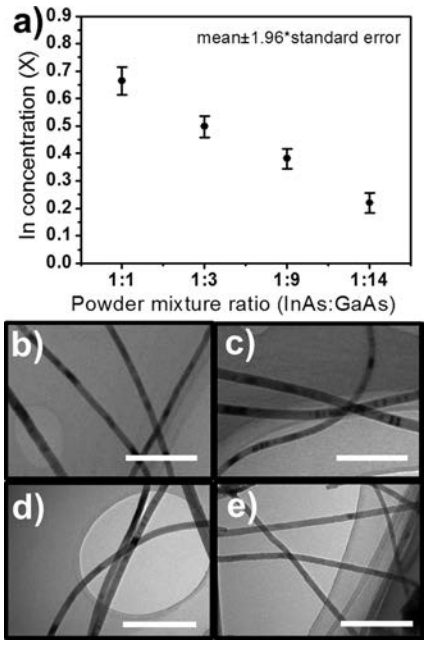

Figure 1. Chemical stoichiometry and surface morphology of the as-grown NWs. (a) In concentration of $In_xGa_{1-x}As$ NWs as a function of the powder mixture ratio. *X* represents the mole fraction of indium. (b–e) TEM images of NWs with average compositions of $In_{0.64}Ga_{0.36}As$, $In_{0.45}Ga_{0.55}As$, $In_{0.3}Ga_{0.7}As$, and $In_{0.22}Ga_{0.78}As$. All scale bars are 200 nm.

statistics of NWs in different composition domains (see Supporting Information Figure S3) have demonstrated a tight control over the NW diameter. By summarizing diameters of 100 NWs for each composition range, we obtained average diameters ranging from 21 to 34 nm (corresponding to plus or minus one standard deviation) for all as-grown NWs utilizing the same catalyst dimensions. The composition-independent diameter here can further eliminate the possibility of excess NW lateral growth under certain stoichiometries and can prepare a consistent platform for a subsequent comparison study among different NW properties. This again highlights the simplicity and potency of our two-step method for the synthesis of uniform, completely composition tunable NWs.

To further shed light on the NW crystal structure, as depicted in Figure 2a, we performed XRD analysis for nine different NW compositions obtained with further control in the NW growth condition in each source powder mixture ratio. The XRD patterns indicate that the grown NWs belong to the cubic zinc blende (ZB) structure, including our pure GaAs and InAs NWs. The peaks correspond to the (111) plane shifting from $2\theta = 25.7°$ (InAs NWs) to $2\theta = 27.1°$ (GaAs NWs) with the plots ordered with decreasing In concentration in between, suggesting the NWs are not phase separated. The full-width at half-maximum (FWHM) of the (111) peaks is ~0.45° and 0.42° for the InAs and GaAs NWs, respectively, while the FWHM values of the (111) peaks for the ternary $In_xGa_{1-x}As$ NWs are all close to ~0.5°, except for the $In_{0.22}Ga_{0.78}As$ NWs of ~0.73°, which can

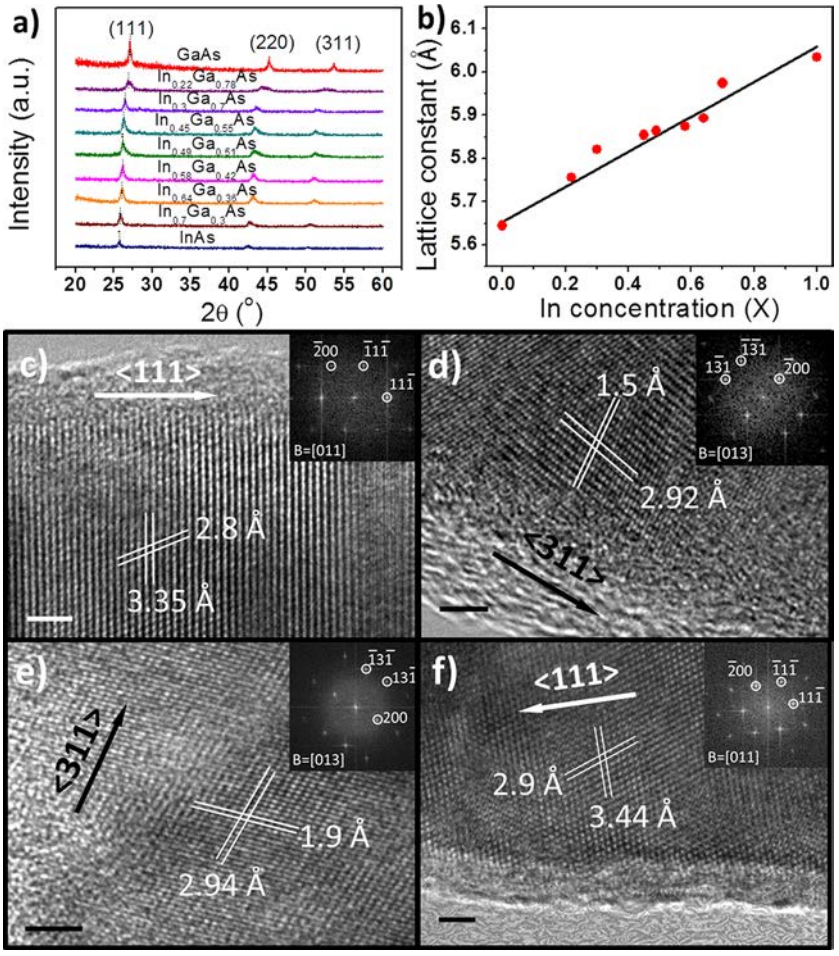

Figure 2. Structural characterizations. (a) XRD patterns of NWs with different chemical compositions including pure InAs, $In_{0.7}Ga_{0.3}As$, $In_{0.64}Ga_{0.36}As$, $In_{0.58}Ga_{0.42}As$, $In_{0.49}Ga_{0.51}As$, $In_{0.45}Ga_{0.55}As$, $In_{0.3}Ga_{0.7}As$, $In_{0.22}Ga_{0.78}As$, and pure GaAs. (b) Red dot: lattice constants, derived from (111) diffraction peak in (a), plotted as a function of In concentration determined by EDS; black solid line: Vegard's law approximation for the $In_xGa_{1-x}As$ NW material system. (c–f) HRTEM of NWs with average compositions of $In_{0.22}Ga_{0.78}As$, $In_{0.3}Ga_{0.7}As$, $In_{0.49}Ga_{0.51}As$, and $In_{0.7}Ga_{0.3}As$. (Inset) Fast Fourier transform images of the NW body showing a cubic ZB structure. All scale bars are 2 nm.

be attributed to the nonoptimized growth conditions in this particular NW stoichiometry. Compared with thin-film $In_xGa_{1-x}As$ materials, the FWHM of NWs is higher, which could arise from the distribution of bond lengths for a random alloy[20] and size-dependent broadening effect.[21] Figure 2b shows the lattice constant determined from the XRD pattern as a function of In concentration. This result (red dots) agrees with Vegard's law approximation in which a near-linear relationship is established between the lattice spacing and NW alloy composition. As the In concentration of NWs increases, the lattice constant increases almost linearly.

In order to demonstrate the detailed structural information of the NW body, high-resolution transmission electron microscopy (HRTEM) was performed for NW samples in different composition domains. As shown in Figure 2c–f, all four NWs exhibit single-crystalline ZB structure. No significant amount of stacking faults or twin-plane polytypic defects were found in these samples; however, the NW growth directions vary among the characterized NWs as presented in Figure 2c–f with the dominant directions in both ⟨111⟩ and ⟨311⟩. Since the NWs are grown randomly on the amorphous substrate, obtaining a mixed growth orientation is not unexpected here.[22] More importantly, the lattice constants concluded from HRTEM images agree well with the results extrapolated from XRD peaks using Bragg's law (see Supporting Information Table S1). Although the lattice constant of $In_{0.28}Ga_{0.72}As$ nanowhiskers is reported as ~5.76 Å,[23] slightly lower than that in our $In_{0.3}Ga_{0.7}As$ NWs, it can be due to the different strain-induced mechanism of the underlying substrates here.[24] Notably, the measurement accuracy in determining lattice constants can be further improved utilizing high-resolution XRD or collecting more HRTEM data in the future; in any case, this highly correlated result suggests that our growth scheme has excellent control over the crystal structure of ternary $In_xGa_{1-x}As$ NWs.

As one of the most important features in ternary NWs, the tunable band gap could be typically determined by photoluminescence (PL) emission[7,25] or optical absorption.[7,26] In this study, we have performed

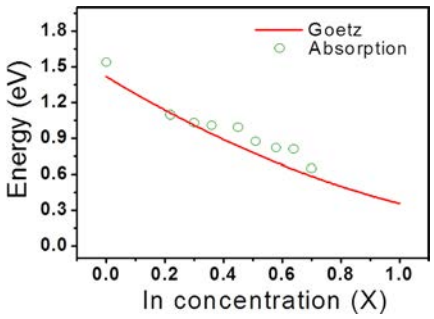

Figure 3. Band gap energy as a function of In concentration. The energy decreases from 1.54 (GaAs NWs) to ~0.65 eV ($In_{0.7}Ga_{0.3}As$ NWs), correspondingly with the bowing function fitted to the experimental data trend.

UV−vis optical absorption measurements to assess the band gap energy for each stoichiometric NW sample (diameters ~25 to 30 nm). As illustrated in Figure 3, the energies were determined from the absorption spectrum (see Supporting Information Figure S4) by linear extrapolation of the absorption edge to zero absorbance. The absorption onset value red-shifts when the In concentration increases (data not shown). It is also noted that the resulting band gap energies follow the same trend as two-dimensional $In_xGa_{1-x}As$ materials.[27] As the In concentration increases, the band gap energy falls from ~1.54 (pure GaAs NWs) to ~0.65 eV ($In_{0.7}Ga_{0.3}As$ NWs); therefore, this manipulation can enable $In_xGa_{1-x}As$ NWs to be used in applications involving wavelengths of 800−1900 nm, such as photodetectors or solar cells. Moreover, most of the band gap values determined here are higher than the bulk values in the literature, which could be attributed to the quantum confinement effect of NWs, leading to larger band gap energies, similar to the previously reported studies of $In_xGa_{1-x}As$ nanocones and nanoparticles.[28] On another hand, by fitting the absorption energy as a function of In composition, a red line is obtained that is similar to the one proposed by Goetz *et al*. with the bowing parameter ($b = -0.475$ eV).[27] Typically, this bowing parameter is a measure of crystal field fluctuation[29] or nonlinear effect[30] arising from the anisotropic binding, and this b value is found to be a lot smaller than those of other reported NW material systems;[31−33] as a result, this relatively small value here suggests that the composition-tunable $In_xGa_{1-x}As$ NW system has a good miscibility without any phase segregation.

In addition to the band gap energies, in order to fully study the electrical behaviors of NW with different chemical stoichiometry, back-gated NW field-effect transistors were fabricated with the same configuration as previously reported.[19] We have performed several thorough statistical studies to quantify the difference among these NW samples. Specifically, we adapt a definition of I_{ON}/I_{OFF} ratio $\approx 10^3$ as the criterion to describe the NW devices being completely turned

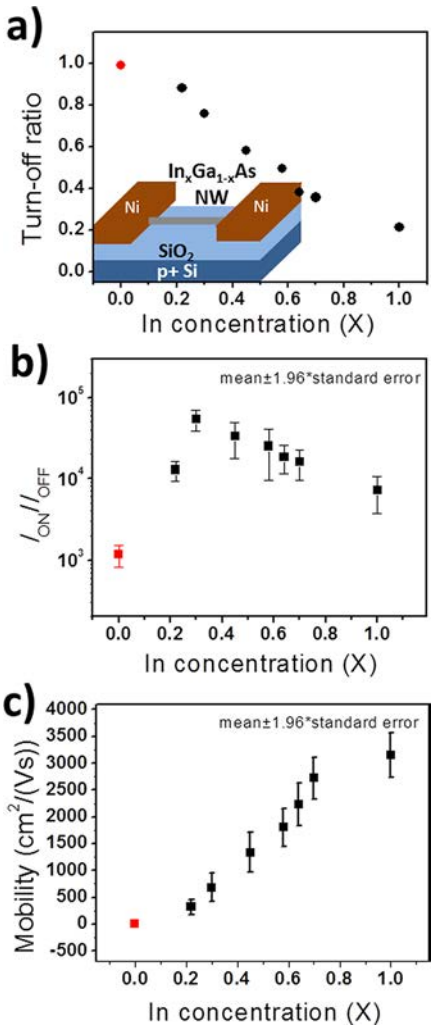

Figure 4. Statistics of the electrical characterization of InGaAs NW-FETs with different NW chemical stoichiometry. (a) Turn-off ratio as a function of In concentration (red dot represents the p-type GaAs NW-FET). (Inset) Schematic of the back-gated NW-FET. (b) I_{ON}/I_{OFF} ratio as a function of In concentration. (c) Field-effect peak electron mobility (hole mobility for the GaAs NW-FET) as a function of In concentration. All NW-FETs have similar channel dimensions for comparison (channel length ~2.5 μm and NW diameter ~25 nm). The mobility was calculated as $V_{DS} = 0.1$ V for all the devices.

off or delivering no current in their "OFF" state. Again, this criterion is chosen on the basis of the typical I_{ON}/I_{OFF} ratio ($\sim 10^3$) reported in state-of-the-art InAs NW devices, and again the main motivation to develop this ternary $In_xGa_{1-x}As$ NW material system is to alleviate the small I_{ON}/I_{OFF} ratio in the small band gap InAs NWs without sacrificing electron mobility.[34,35] In this case, the so-called "turn-off ratio" is calculated as the number of turn-off devices divided by the total number of ~100 devices measured in each NW stoichiometry. As shown in Figure 4a, the turn-off ratio is the highest for the p-type GaAs NW-FET (red color) and then decreases gradually as the In concentration increases. This reduction probably corresponds to the decreased band gap of In-rich NWs, which can lead to a significant amount

of leakage current, and thus it is harder to completely turn off the devices. For a fair and consistent comparison, the same thickness (0.5 nm) of catalytic Au film was used in each NW synthesis so that the diameter-dependent electrical properties of the NWs can be eliminated here. Moreover, among all turn-off NW-FETs and based on a statistic of more than 50 devices, as the In concentration increases from 20% to 100%, the I_{ON}/I_{OFF} ratio decreases accordingly, which suggests that the lowering of the band gap indeed deteriorates the off-state leakage (Figure 4b). Notably, for the p-type GaAs and n-type $In_{0.22}Ga_{0.78}As$ NW-FETs, the ON-current is observed to be quite low, usually in the several hundreds of pA or several tens of nA range; despite the high turn-off ratio and low OFF-current due to the band gap opening, the corresponding I_{ON}/I_{OFF} ratio would not be as high as compared with other stoichiometric devices. Furthermore, as depicted in Figure 4c, the statistic of field-effect electron mobility (hole for the pure GaAs NW-FET) shows the nearly monatomic increase from Ga-rich devices (averaging ~320 $cm^2/(V\cdot s)$) to In-rich devices (averaging ~2700 $cm^2/(V\cdot s)$). Transfer characteristics of NW-FETs were used to calculate the field-effect mobility as previously described (see Supporting Information Figure S5).[19] This increase in mobility corresponds to the reduction in the band gap and I_{ON}/I_{OFF} ratio and an increase in the In concentration. In addition, considering the previously reported size modulation of electrical behaviors of NW-FET,[36] we may further manipulate the electrical behavior of our devices with different NW diameters. In any case, all these findings have provided a design guideline in the chemical stoichiometric selection of ternary NWs in which the enhancement of the I_{ON}/I_{OFF} ratio may be attained only at the cost of field-effect mobility degradation, therefore requiring careful considerations for achieving optimal device performance.

CONCLUSION

Utilizing a simple two-step growth method, we have demonstrated the ability to tune the composition and band gap of single-crystalline ternary $In_xGa_{1-x}As$ NWs across the entire alloy range by manipulating the source powder mixture ratio as well as the growth conditions. Importantly, the as-grown NWs exhibit a well-controlled surface morphology and low defect concentration without any phase segregation in all stoichiometric composition domains. Through summarizing the electrical behaviors of back-gated $In_xGa_{1-x}As$ NW-FETs, we found that statistically when the In concentration increases, due to the reduction in the band gap, the turn-off ratio and I_{ON}/I_{OFF} ratio decrease, but the field-effect mobility is enhanced monotonically. All these stoichiometric-dependent electrical characteristics have served as an essential guideline for device material design and performance considerations of high-performance ternary NWs.

METHODS

Nanowire Synthesis. To synthesize $In_xGa_{1-x}As$ NWs with different chemical stoichiometry, InAs and GaAs source powder in various mixture ratios (1:1, 1:3, 1:9, and 1:14 in wt %) were loaded in a boron nitride crucible. The growth substrates were SiO_2/Si wafer pieces with 50 nm thick thermal oxide on the top. Au thin films of 0.5 nm thickness were used as the catalysts for all NW growth. Considering the different evaporation velocity of source powders, different source temperatures were used for each mixture ratio. For example, for a 1:1 mixture, 800 °C was used, while for a 1:9 mixture, 850 °C was used for the source temperature. The growth temperatures, including both nucleation and growth steps, were adjusted carefully as well to produce the highly crystalline NWs. For example, for the 1:3 mixture, the nucleation temperature was set at 620 °C and growth temperature at 550 °C while for the 1:14 mixture, the temperatures were 650 and 580 °C, respectively.

Material Characterizations. All material characterizations were performed on the NWs obtained in the 0−1 cm region of growth substrates in order to establish a consistent study on the chemical stoichiometry. Specifically, the XRD characterization was carried out in a Philips powder diffractometer using Cu Kα radiation. The scanning step was set to be 0.001°, and each step time was 1 s in order to increase the accuracy of the measurement. To resolve the lattice constant, we first obtained the position of the (111) peak from the XRD pattern, which is essentially the value of 2θ. Then we applied Bragg's law: $n\lambda = 2d_{hkl} \sin\theta$ with $\lambda = 1.54$ Å. From the d_{hkl} value that we calculated, the lattice constant could be calculated by d times $\sqrt{(h^2 + k^2 + l^2)}$. The SEM images were taken from an FEI/Philips XL30 scanning electron microscope, and TEM images were taken using a Philips CM-20 transmission electron microscope. HRTEM images were observed with a JEOL 2100F transmission electron microscope. To prepare the TEM samples, NWs were first harvested in high-purity ethanol solution and then drop-casted on a Cu grid. The UV−vis optical absorption measurement was performed in an ultraviolet−visible−near infrared spectrophotometer with an integrating sphere (PE Lamda 750).

Conflict of Interest: The authors declare no competing financial interest.

Acknowledgment. This research was supported by the City University of Hong Kong (Project No. 9610214).

Supporting Information Available: Comparison of NW lattice constants obtained from HRTEM *versus* XRD; SEM images of the NWs with different chemical compositions; representative EDS spectra within the NW body; NW diameter statistics; selected UV-vis absorption of $In_{0.49}Ga_{0.51}As$ NW; and electrical transfer characteristics of NW FETs. These materials are available free of charge *via* the Internet at http://pubs.acs.org.

REFERENCES AND NOTES

1. Cui, Y.; Lieber, C. M. Functional Nanoscale Electronic Devices Assembled Using Silicon Nanowire Building Blocks. *Science* **2001**, *291*, 851–853.
2. Chan, C. K.; Peng, H. L.; Liu, G.; McIlwrath, K.; Zhang, X. F.; Huggins, R. A.; Cui, Y. High-Performance Lithium Battery Anodes Using Silicon Nanowires. *Nat. Nanotechnol.* **2008**, *3*, 31–35.
3. Duan, X. F.; Huang, Y.; Cui, Y.; Wang, J. F.; Lieber, C. M. Indium Phosphide Nanowires as Building Blocks for

Nanoscale Electronic and Optoelectronic Devices. *Nature* **2001**, *409*, 66–69.
4. Yan, R. X.; Gargas, D.; Yang, P. D. Nanowire Photonics. *Nat. Photonics* **2009**, *3*, 569–576.
5. Lim, S. K.; Tambe, M. J.; Brewster, M. M.; Gradecak, S. Controlled Growth of Ternary Alloy Nanowires Using Metalorganic Chemical Vapor Deposition. *Nano Lett.* **2008**, *8*, 1386–1392.
6. Sharma, G.; Mor, G. K.; Varghese, O. K.; Paulose, M.; Grimes, C. A. Synthesis and Characterization of Extremely Uniform Fe-Co-Ni Ternary Alloy Nanowire Arrays. *J. Nanosci. Nanotechnol.* **2004**, *4*, 738–743.
7. Kuykendall, T.; Ulrich, P.; Aloni, S.; Yang, P. Complete Composition Tunability of InGaN Nanowires Using a Combinatorial Approach. *Nat. Mater.* **2007**, *6*, 951–956.
8. He, C. Y.; Wu, Q. A.; Wang, X. Z.; Zhang, Y. L.; Yang, L. J.; Liu, N.; Zhao, Y.; Lu, Y. N.; Hu, Z. Growth and Characterization of Ternary AlGaN Alloy Nanocones across the Entire Composition Range. *ACS Nano* **2011**, *5*, 1291–1296.
9. Junpeng, L.; Cheng, S.; Minrui, Z.; Mathews, N.; Hongwei, L.; Seng, C. G.; Xinhai, Z.; Mhaisalkar, S. G.; Haur, S. C. Facile One-Step Synthesis of CdS_xSe_{1-x} Nanobelts with Uniform and Controllable Stoichiometry. *J. Phys. Chem. C* **2011**, *115*, 19538–19545.
10. Pan, A. L.; Zhou, W. C.; Leong, E. S. P.; Liu, R. B.; Chin, A. H.; Zou, B. S.; Ning, C. Z. Continuous Alloy-Composition Spatial Grading and Superbroad Wavelength-Tunable Nanowire Lasers on a Single Chip. *Nano Lett.* **2009**, *9*, 784–788.
11. Yan, C. Y.; Singh, N.; Lee, P. S. Wide-Bandgap Zn_2GeO_4 Nanowire Networks as Efficient Ultraviolet Photodetectors with Fast Response and Recovery Time. *Appl. Phys. Lett.* **2010**, *96*, 053108.
12. Yang, Y.; Sun, X. W.; Tay, B. K.; Wang, J. X.; Dong, Z. L.; Fan, H. M. Twinned Zn_2TiO_4 Spinel Nanowires Using ZnO Nanowires as a Template. *Adv. Mater.* **2007**, *19*, 1839–1844.
13. Lin, Y. F.; Hsu, Y. J.; Lu, S. Y.; Chen, K. T.; Tseng, T. Y. Well-Aligned Ternary $Cd_{1-x}Zn_xS$ Nanowire Arrays and Their Composition-Dependent Field Emission Properties. *J. Phys. Chem. C* **2007**, *111*, 13418–13426.
14. Fuchi, S.; Nonogaki, Y.; Moriya, H.; Koizumi, A.; Fujiwara, Y.; Takeda, Y. Composition Dependence of Energy Structure and Lattice Structure in InGaAs/GaP. *Phys. E* **2004**, *21*, 36–44.
15. Huang, M. L.; Chang, Y. C.; Chang, C. H.; Lin, T. D.; Kwo, J.; Wu, T. B.; Hong, M. Energy-Band Parameters of Atomic-Layer-Deposition Al_2O_3/InGaAs Heterostructure. *Appl. Phys. Lett.* **2006**, *89*, 012903.
16. Jenichen, A.; Engler, C. Stability and Band Gaps of InGaAs, BGaAs, and BInGaAs Alloys: Density-Functional Supercell Calculations. *Phys. Status Solidi B* **2007**, *244*, 1957–1963.
17. Shin, J. C.; Kim, K. H.; Yu, K. J.; Hu, H. F.; Yin, L. J.; Ning, C. Z.; Rogers, J. A.; Zuo, J. M.; Li, X. L. $In_xGa_{1-x}As$ Nanowires on Silicon: One-Dimensional Heterogeneous Epitaxy, Bandgap Engineering, and Photovoltaics. *Nano Lett.* **2011**, *11*, 4831–4838.
18. Jung, C. S.; Kim, H. S.; Jung, G. B.; Gong, K. J.; Cho, Y. J.; Jang, S. Y.; Kim, C. H.; Lee, C. W.; Park, J. Composition and Phase Tuned InGaAs Alloy Nanowires. *J. Phys. Chem. C* **2011**, *115*, 7843–7850.
19. Hou, J. J.; Han, N.; Wang, F.; Xiu, F.; Yip, S.; Hui, A. T.; Hung, T.; Ho, J. C. Synthesis and Characterizations of Ternary InGaAs Nanowires by a Two-Step Growth Method for High-Performance Electronic Devices. *ACS Nano* **2012**, *6*, 3624–3630.
20. Mattila, T.; Zunger, A. Predicted Bond Length Variation in Wurtzite and Zinc-Blende InGaN and AlGaN Alloys. *J. Appl. Phys.* **1999**, *85*, 160–167.
21. Ptatschek, V.; Schreder, B.; Herz, K.; Hilbert, U.; Ossau, W.; Schottner, G.; Rahauser, O.; Bischof, T.; Lermann, G.; Materny, A.; *et al.* Sol-Gel Synthesis and Spectroscopic Properties of Thick Nanocrystalline CdSe Films. *J. Phys. Chem. B* **1997**, *101*, 8898–8906.
22. Han, N.; Hui, A. T.; Wang, F. Y.; Hou, J. J.; Xiu, F.; Hung, T. F.; Ho, J. C. Crystal Phase and Growth Orientation Dependence of GaAs Nanowires on Ni_xGa_y Seeds *via* Vapor-Solid-Solid Mechanism. *Appl. Phys. Lett.* **2011**, *99*, 083114.
23. Regolin, I.; Khorenko, V.; Prost, W.; Tegude, F. J.; Sudfeld, D.; Kastner, J.; Dumpich, G. Composition Control in Metal-Organic Vapor-Phase Epitaxy Grown InGaAs Nanowhiskers. *J. Appl. Phys.* **2006**, *100*, 074321.
24. Tomioka, K.; Tanaka, T.; Hara, S.; Hiruma, K.; Fukui, T. III-V Nanowires on Si Substrate: Selective-Area Growth and Device Applications. *IEEE J. Sel. Top. Quantum Electron.* **2011**, *17*, 1112–1129.
25. Wang, X. D.; Song, J. H.; Li, P.; Ryou, J. H.; Dupuis, R. D.; Summers, C. J.; Wang, Z. L. Growth of Uniformly Aligned ZnO Nanowire Heterojunction Arrays on GaN, AlN, and $Al_{0.5}Ga_{0.5}N$ Substrates. *J. Am. Chem. Soc.* **2005**, *127*, 7920–7923.
26. Li, L.; Yang, Y. W.; Huang, X. H.; Li, G. H.; Zhang, L. D. Fabrication and Characterization of Single-Crystalline ZnTe Nanowire Arrays. *J. Phys. Chem. B* **2005**, *109*, 12394–12398.
27. Goetz, K. H.; Bimberg, D.; Jurgensen, H.; Selders, J.; Solomonov, A. V.; Glinskii, G. F.; Razeghi, M. Optical and Crystallographic Properties and Impurity Incorporation of $Ga_XIn_{1-X}As$ ($0.44 < X < 0.49$) Grown by Liquid-Phase Epitaxy, Vapor-Phase Epitaxy, and Metal Organic-Chemical Vapor-Deposition. *J. Appl. Phys.* **1983**, *54*, 4543–4552.
28. Guisbiers, G.; Abudukelimu, G.; Wautelet, M.; Buchaillot, L. Size, Shape, Composition, and Segregation Tuning of InGaAs Thermo-Optical Properties. *J. Phys. Chem. C* **2008**, *112*, 17889–17892.
29. Chichibu, S. F.; Abare, A. C.; Minsky, M. S.; Keller, S.; Fleischer, S. B.; Bowers, J. E.; Hu, E.; Mishra, U. K.; Coldren, L. A.; DenBaars, S. P.; *et al.* Effective Band Gap Inhomogeneity and Piezoelectric Field in InGaN/GaN Multiquantum Well Structures. *Appl. Phys. Lett.* **1998**, *73*, 2006–2008.
30. Agrawal, B. K.; Yadav, P. S.; Srivastava, R.; Agrawal, S. *Ab Initio* Study of Anomalous Band-Gap Bowing in $GaAs_{1-x}N_x$ Alloys. *J. Phys.-Condes. Matter* **1998**, *10*, 4597–4607.
31. Kuo, Y. K.; Chu, H. Y.; Yen, S. H.; Liou, B. T.; Chen, M. L. Bowing Parameter of Zincblende $In_xGa_{1-x}N$. *Opt. Commun.* **2007**, *280*, 153–156.
32. Oh, T. S.; Lee, Y. S.; Jeong, H.; Di Kim, J.; Seo, T. H.; Suh, E. K. Large-Bandgap Bowing of $In_xAl_{1-x}N$ Ternary Films Grown by Using Metalorganic Chemical Vapor Deposition. *J. Korean Phys. Soc.* **2008**, *53*, 1956–1960.
33. Azzi, S.; Zaoui, A.; Ferhat, M. On the Importance of the Band Gap Bowing in Boron-Based III-V Ternary Alloys. *Solid State Commun.* **2007**, *144*, 245–248.
34. Jiang, X. C.; Xiong, Q. H.; Nam, S.; Qian, F.; Li, Y.; Lieber, C. M. InAs/InP Radial Nanowire Heterostructures as High Electron Mobility Devices. *Nano Lett.* **2007**, *7*, 3214–3218.
35. Lind, E.; Persson, A. I.; Samuelson, L.; Wernersson, L. E. Improved Subthreshold Slope in an InAs Nanowire Heterostructure Field-Effect Transistor. *Nano Lett.* **2006**, *6*, 1842–1846.
36. Han, N.; Wang, F.; Hou, J. J.; Xiu, F.; Yip, S.; Hui, A. T.; Hung, T.; Ho, J. C. Controllable p–n Switching Behaviors of GaAs Nanowires via an Interface Effect. *ACS Nano* **2012**, *6*, 4428–4433.